Supporting information

NiFeCo-OH/NiTe nanoarrays with amorphous/crystalline interfaces for highly efficient oxygen evolution reaction

Jing Liu[a], Da Liu[a], Xiaoxiao Yan[a], Peifang Guo[a], Hongbin Xu[b], Peng Chen[a], and Renbing Wu*[a]

[a] Department of Materials Science, Fudan University, Shanghai, 200433, China

[b] Department of Materials Science and Engineering, Massachusetts Institute of Technology; Cambridge, MA 02139, USA

Experimental sections

Chemical and reagents

Nickel nitrate hexahydrate ($Ni(NO_3)_2 \cdot 6H_2O$, 99%), Cobalt nitrate hexahydrate ($Co(NO_3)_2 \cdot 6H_2O$, 99%), Ferric nitrite nonahydrate ($Fe(NO_3)_3 \cdot 9H_2O$, 99%), Sodium tellurite ($NaTeO_3$, 99.9%) were obtained from Aladdin Chemical Reagent Co., Ltd. Hydrazine hydrate ($N_2H_4 \cdot H_2O$, 50%) was bought from China National Pharmaceutical Group Corporation. All chemicals were of analytical grade and used as received without further purification. The deionized water (18 MΩ cm^{-1}) used in all experiments was purified through a Millipore system.

Synthesis of NiTe@NF

Before any reaction process, the nickel foam was immersed in 1 M HCl for 1 h, and then washed with deionized water and ethanol in sequence for several times. The reaction solution was prepared through dissolving $NaTeO_3$ (443 mg, 2 mmol) in 20 mL water and then mixing with $N_2H_4 \cdot H_2O$ (36 mL), which was continuously stirred for 1 h to make sure homogeneity. Then, a piece of well-prepared nickel foam (NF, 4 cm × 4 cm) was immersed in the as-prepared solution and successively sealed in the Teflon-lined autoclave heating at 180°C for 16 h. Finally, the resultant NiTe arrays in-situ growing onto NF (NiTe@NF) was taken out from the autoclave and washed with deionized water and ethanol in sequence for several times, and finally dried under 60°C overnight.

Synthesis of NiFeCo-OH/NiTe@NF, NiFeCo-OH@NF, NiFe-OH/NiTe@NF and NiFe-OH@NF

All the hydroxides were synthesized by electrodeposition methods using a standard three-electrode system with the saturated calomel electrode (SCE), a graphite rod and the NiTe@NF as the reference electrode, counter electrode and working electrode,

respectively. The mechanism could be generally interpreted that cathodic reactions at the working electrode resulted in the increase of local pH value near the electrode surface and numerous OH^- ions were generated. Successively, metal ions in the solution were kinetically deposited with OH^- to form hydroxides.[1,2]

The electrolyte for NiFeCo-hydroxides was prepared through dissolving 0.06 M $Ni(NO_3)_2 \cdot 6H_2O$, 0.02 M $Fe(NO_3)_3 \cdot 9H_2O$ and 0.02 M $Co(NO_3)_2 \cdot 6H_2O$ in 100 mL water with continuously stirring for 10 mins. The NiFeCo-hydroxides were electrochemically deposited on the surface of bare NiTe@NF, blank NF (0.5 cm × 0.5 cm) at −1.2 V *vs.* SCE for 90 s in the mixed aqueous solution, which was denoted as NiFeCo-OH/NiTe@NF and NiFeCo-OH@NF, respectively. Finally, the catalysts were taken out from the mixed solution and washed with distilled water and ethanol in sequence for several times, and then dried under 60℃ overnight. Similarly, the NiFe-OH/NiTe@NF, NiFe-OH@NF were prepared with the same parameters except the electrolyte not containing $Co(NO_3)_2 \cdot 6H_2O$.

Synthesis of NiFeCo-OH/NiTe@NF-*c*-*t*

The other contrast catalysts were prepared by different electrodeposition durations (t = 30 s, 90 s, 180 s) and with different deposition solutions containing 0.01 M, 0.02 M and 0.03 M $Co(NO_3)_2 \cdot 6H_2O$ (c = 1, 2, 3), denoted as NiFeCo-OH/NiTe@NF-*c*-*t*.

Materials characterizations

The test of scanning electron microscope (SEM) was conducted on a field-emission scanning electron microscopy (FESEM, Ultra 55, Zeiss, Germany). The test of transmission electron microscopy (TEM), high resolution TEM (HRTEM) analysis coupled with energy dispersive spectroscopy (EDS) was collected on a JEOL-2100F, FEI-Talos F200S transmission electron microscope operating at 200 kV, respectively. XRD patterns were collected over the 2θ range of 10–70º on a Bruker D8 Focus X-ray

diffractometer equipped with a Cu Kα radiation source (λ = 1.5405 Å). Fourier Transform Infrared Spectrometer (FT-IR) was (4000–800 cm^{-1}) were obtained by Thermo Nicolet IS 20. The surface elemental composition was studied through X-ray photoelectron spectroscopy (XPS, Thermo Scientific Escalab Xi+) using the Al K_α line as the excitation source. Besides, the soft X-ray absorption spectroscopy (XAS) in total electron yield (TEY) mode was performed at the BL10B beamline in national synchrotron radiation laboratory (NSRL) and the samples were prepared by the powder scraped from the surface of NiFeCo-OH/NiTe@NF, NiFe-OH/NiTe@NF, NiTe@NF. Inductively coupled plasma atomic emission spectroscopy (ICP-AES, Thermo Scientific iCAP 7400) was used to quantify the amount of Ni, Fe, Co, Te in the sample of NiFeCo-OH/NiTe scraped from the nickel foam.

Electrochemical measurements

All the electrochemical measurements were conducted on the CHI 760E electrochemical workstation (CH Instruments, Inc., Shanghai) using a typical three-electrode configuration in 1.0 M KOH solution. The saturated calomel electrode (SCE), graphite rod and the catalysts supported on nickel foam were used as the reference electrode, counter electrode and working electrode, respectively. The linear sweep voltammetry (LSV) polarization curves for OER were scanned at the scan rate of 5 mV s^{-1} at room temperature. The long-term measurements were performed with chronoamperometry at the potential of 1.52 V *vs.* RHE. All the measured polarization curve potentials were performed with iR compensation and were converted to reverse hydrogen electrode (RHE) by the calibration equation (E *vs.* RHE = E *vs.* SCE + 0.2415 V + 0.05916 pH – iR_s). The electrochemical impedance spectroscopy (EIS) was carried out in the frequency range of 0.01 Hz ~100 kHz at the potential of 1.56 V *vs.* RHE in 1.0 M KOH solution for OER. The cyclic voltammetry (CV) curves of the samples

were collected in 1.0 M KOH solution from 1 V to 1.05 V *vs.* RHE for OER at varying scan rates (20, 40, 60, 80, and 100 mV s^{-1}) and there are no evident redox processes occurred in this potential range. The ECSA was calculated by the equation (ECSA = C_{dl} / C_s), where C_s was a constant of 0.04 mF cm^{-2} in the literature[3].

Desnsity functional theory calculations

Density functional theory calculations plus Hubbard-U and dispersion interactions (i.e., van der Waals effects) (DFT + U + vdW) were conducted with the Perdew-Burke-Ernzenhof (PBE) as a generalized gradient approximation (GGA) method to obtain exchange correlation functional and projector-augmented wave (PAW) pseudopotentials employed in calculation, as implemented in the Vienna Ab initio Simulation Package (VASP) code.[4,5] The Hubbard-U correction (DFT+U method) was applied to improve the description of localized metal d-electrons in the corresponding oxyhydroxides systems. The values of U-J terms were set as 6.0 for Ni cations to correct the relative strong interaction of electrons in 3*d* orbitals of transition metals.[6, 7] All calculations were spin-polarized. The heterostructure is biult through junction of (010) suface of NiTe and (100) surface of FeCoNi-OOH with lattice mismatch less than 5%. A vacuum layer with thickness of 20 Å was built on the surface of (001) in both NiTe-oxyhydroxides heterostructures and oxyhydroxides systems and a vacuum space to avoid interactions along the z direction. In addition, (001)-surface slabs of individual NiTe and FeCoNi-OOH with vacuum layer of 20 Å were also built for oxygen evolution reaction caculations. Van der Waals effects in the system were applied using Grimme's DFT-D3 (B-J) correction method, and dipole corrections along the surface normal were taken into account. Brillouin zone sampling was conducted using a Γ-centered Monkhorst-Pack grid with 3 × 3 × 1 k-point mesh. The wave functions of valence electrons were expanded using a plane wave basis set with a cut-off energy of 500 eV.

The convergence criterion for energy was 10^{-6} eV between two electronic steps. For structural optimization loop, the maximum force on each atom was less than −0.01 eV/Å.

Gibbs free energy calculation

The four steps involved in OER proposed by Nørskov et. al.[8] on transition metal compounds are listed in supplementary equations (1) to (4) below:

$$OH^- + * \rightarrow M^*OH + e^- \quad (1)$$

$$M^*OH + OH^- \rightarrow M^*O + H_2O\ (l) + e^- \quad (2)$$

$$M^*O + OH^- \rightarrow M^*OOH + e^- \quad (3)$$

$$M^*OOH + OH^- \rightarrow M^* + O_2\ (g) + H_2O\ (l) + e^- \quad (4)$$

Here, we applied a method previously developed for modeling the thermochemistry of electrochemical reactions based on density functional calculations. In this method, Gibbs free energy was used as a descriptor to evaluate whether reactions proceed spontaneously. Specifically, the Gibbs free energy can be obtained by adding corrections including entropic (TS) and zero-point energy (ZPE) contributions to the calculated DFT energy, and the Gibbs free energy for each step can be calculated by as following:

$$\Delta G = \Delta E_{DFT} + \Delta ZPE - T\Delta S \quad (5)$$

Where the E_{DFT} is the calculated DFT energy of corresponding systems, ΔZPE is the change in ZPE calculated from the vibrational frequencies and ΔS is the change in the entropy sourced from thermodynamics databases. For gas phase molecule, the entropy term can be expressed as the sum of the translational, rotational, and vibrational contributions, whereas for adsorbates the translational and rotational entropy were not taken into account due to negligible contributions. Specifically, the vibration frequency

of hydrogen adsorption is 3211.45 cm^{-1}, which is not sensitive to the adsorption sites. The entropy is obtained based on the equation:

$$S(T) = \sum_{i=1}^{3N} \left[-R\ln\left(1 - e^{-\frac{hv_i}{k_B T}}\right) + \frac{N_A h v_i \; e^{-hv_i/k_B T}}{T \; 1 - e^{-hv_i/k_B T}} \right] \quad (6)$$

where R stands for the universal gas constant, k_B is the Boltzmann constant, h is Plank's constant, N_A is Avogadro's number, v_i represents the frequency and N is the number of adsorbed atoms. In addition, during these frequency computations, all atoms of substrate were rigidly constrained so that no additional degrees of freedom from catalysts are introduced into the reaction system. Therefore, such calculations were performed just for the reaction intermediates, and the contributions from the catalysts to ΔE_{ZPE} and ΔS are neglected. In addition, the relation that Gibbs free energy of a proton (G_{H+}) equals to that of the half of a hydrogen molecule in gaseous H_2 ($1/2G_{H2}$) was used in every step of electrochemical reactions containing electron transfer. Since energy of the triplet state of the O_2 molecule was hardly to precisely acquire through current DFT procedures, the free energy of the O_2 molecule was calculated according to $G_{O2} = 2G_{H2O} - 2G_{H2} + 4.92$ eV. The adsorption free energy of different intermediate species involved in OER process could therefore be described by the equations below:

$$\Delta G_{*OH} = G_{*OH} + 1/2G_{H2} - G^* - G_{H2O} \quad (7)$$

$$\Delta G_{*O} = G_{*O} + G_{H2} - G^* - G_{H2} \quad (8)$$

$$\Delta G_{*OOH} = G_{*OOH} + 3/2G_{H2} - G^* - 2G_{H2O} \quad (9)$$

Therefore, the reaction free energies of equations (7–9) can be obtained from the adsorption free energies of the oxygen-containing intermediates formed during OER (the item of U represets applied potential at the sacle of reversible hydrogen electrode):

$$\Delta G_1 = \Delta G_{*OH} - eU \quad (10)$$

$$\Delta G_2 = \Delta G_{*O} - \Delta G_{*OH} - eU \quad (11)$$

$$\Delta G_3 = \Delta G_{*OOH} - \Delta G_{*O} - eU \quad (12)$$

$$\Delta G_4 = 4.92\ eV - \Delta G_{*OOH} - eU \quad (13)$$

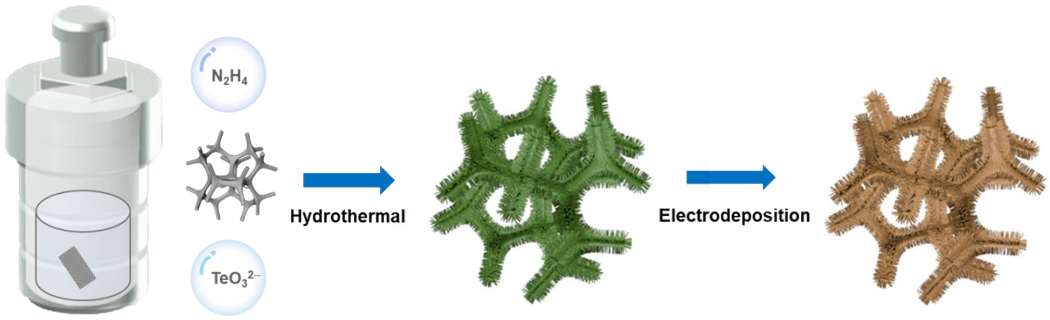

Scheme S1. Schematic illustration of the synthesis of NiFeCo-OH/NiTe@NF.

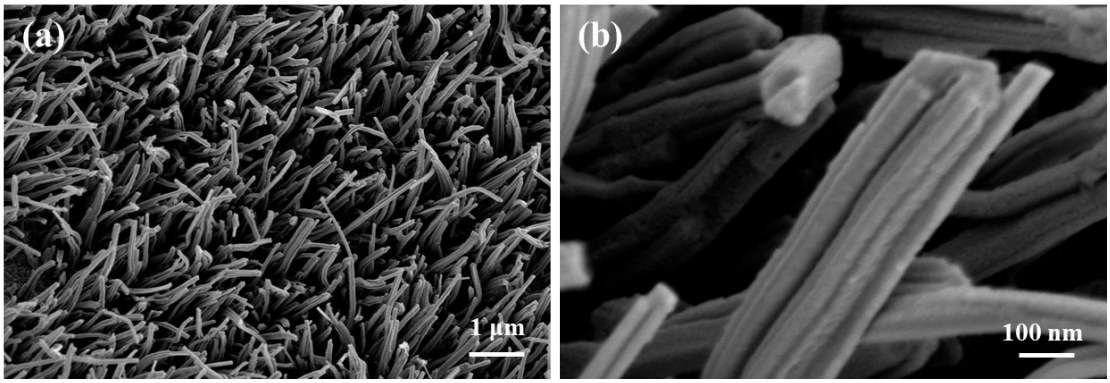

Fig.S1. FESEM images of NiTe@NF.

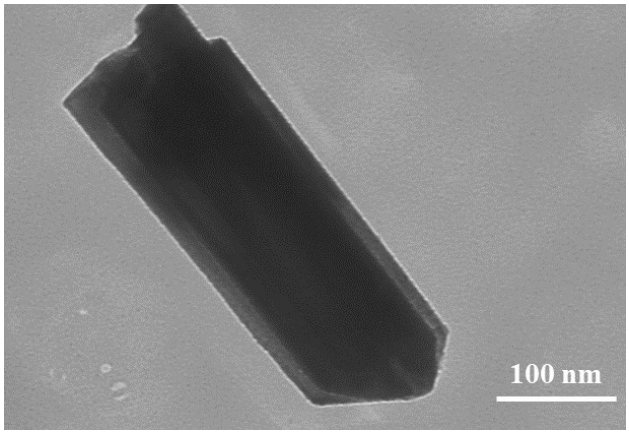

Fig. S2. TEM image of NiTe@NF.

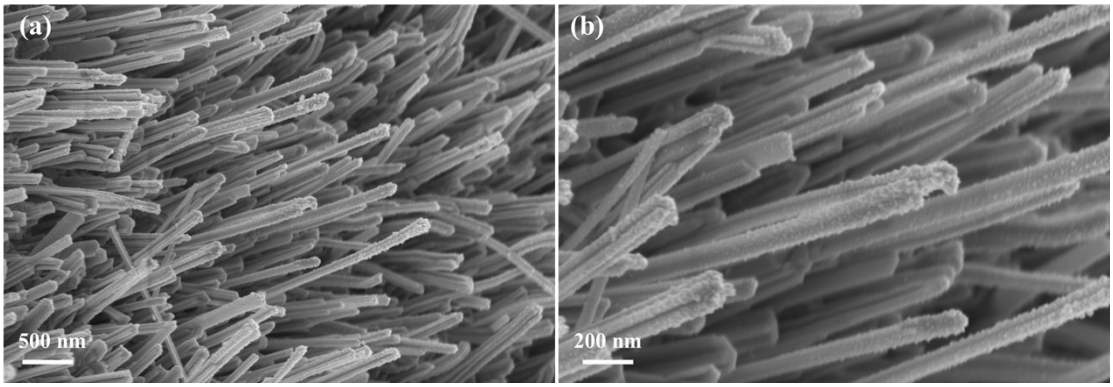

Fig. S3. FESEM images of NiFe-OH/NiTe@NF.

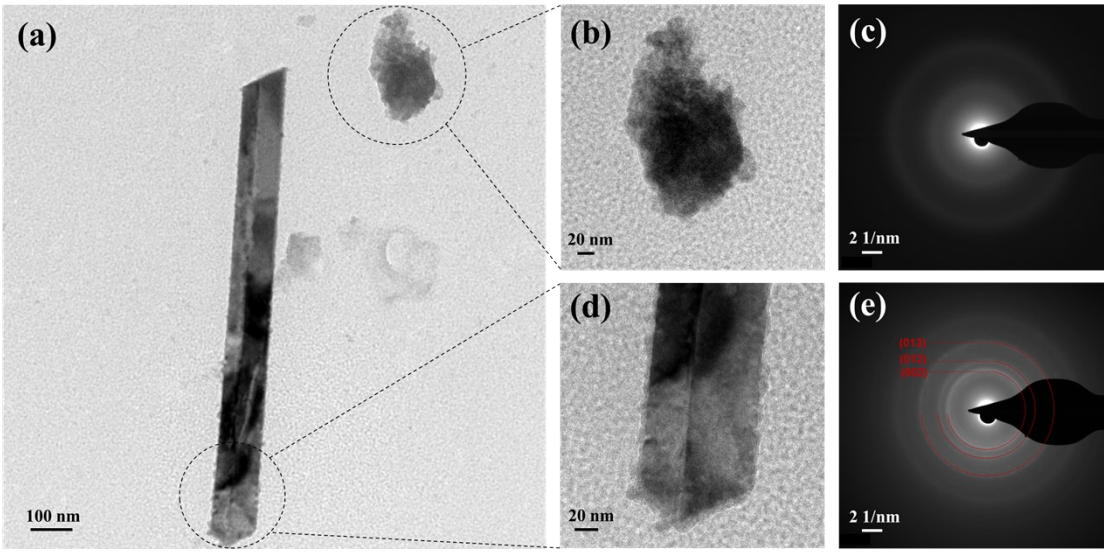

Fig. S4. (a) and (d) TEM images of NiFeCo-OH/NiTe and (e) the corresponding SAED pattern. (b) TEM image of the agglomerated NiFeCo-hydroxides falling off the nanorods by ultrasonic treatment and (c) the corresponding SAED pattern.

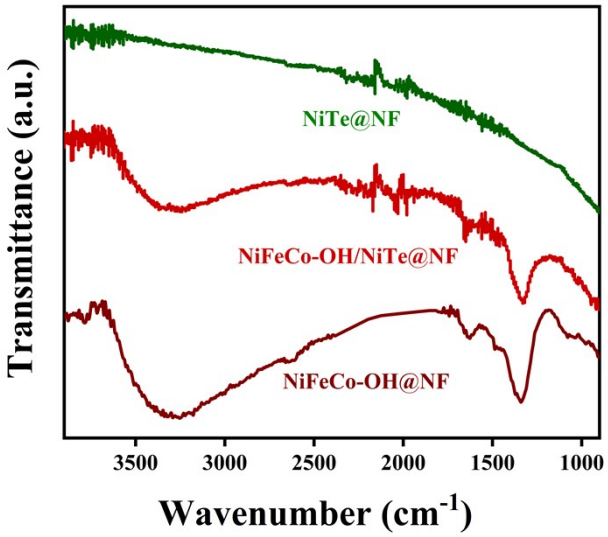

Fig. S5. FT-IR spectroscopy of NiTe@NF, NiFeCo-OH/NiTe@NF and NiFeCo-OH@NF.

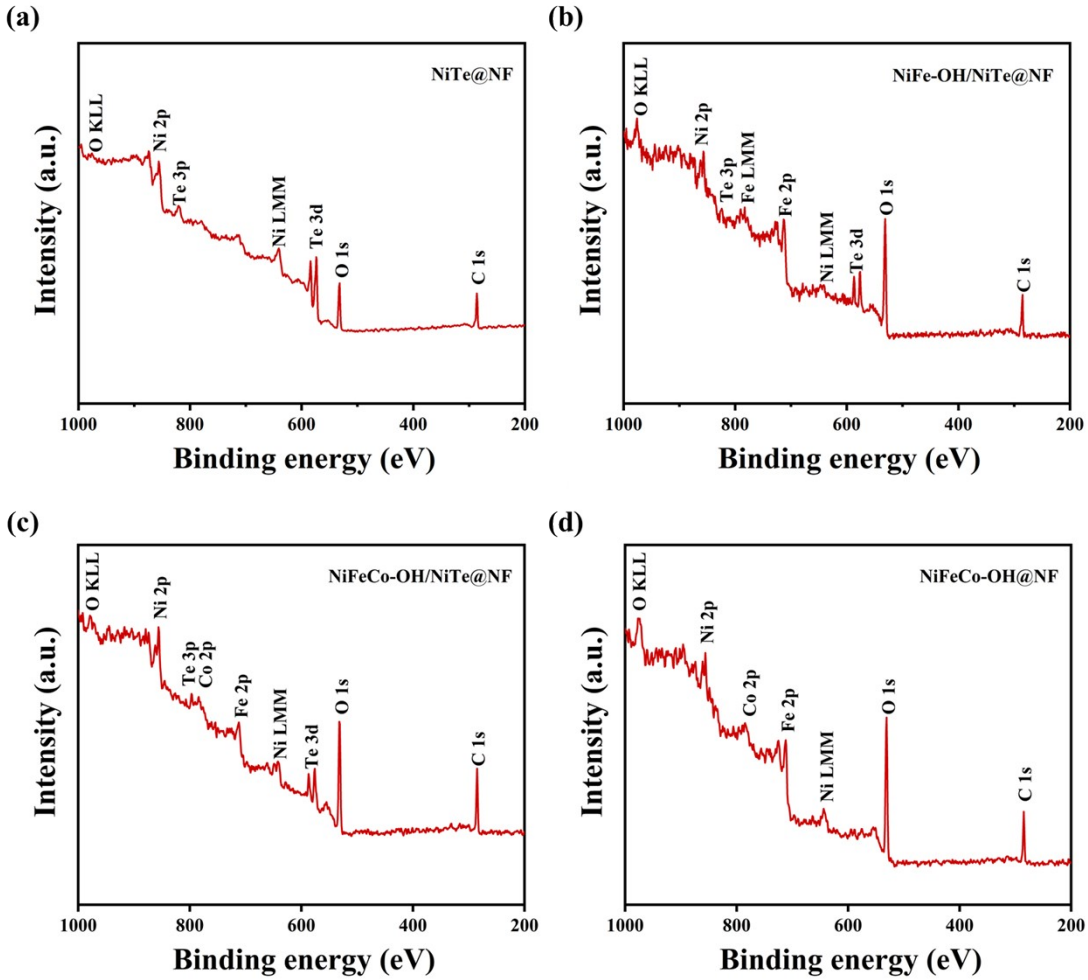

Fig. S6. XPS survey spectra of (a) NiTe@NF, (b) NiFe-OH/NiTe@NF, (c) NiFeCo-OH/NiTe@NF and (d) NiFeCo-OH@NF.

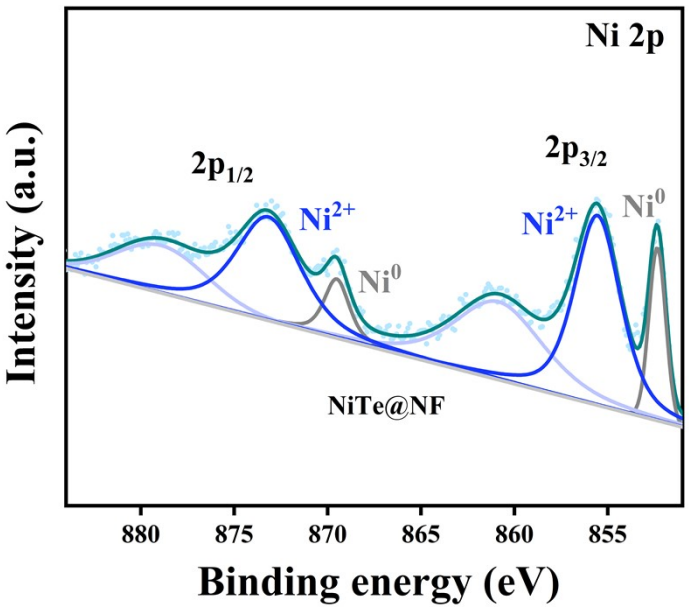

Fig. S7. High-resolution Ni 2p XPS spectra of NiTe@NF.

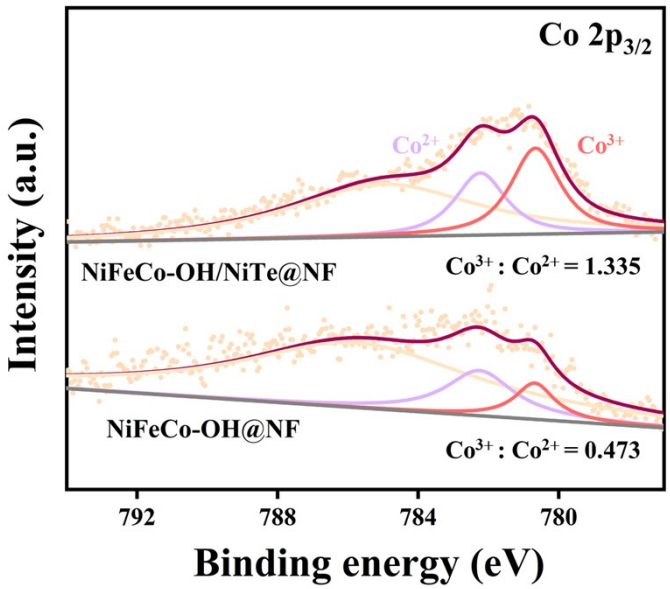

Fig. S8. High-resolution Co 2p XPS spectra of NiFeCo-OH/NiTe@NF and NiFeCo-OH@NF.

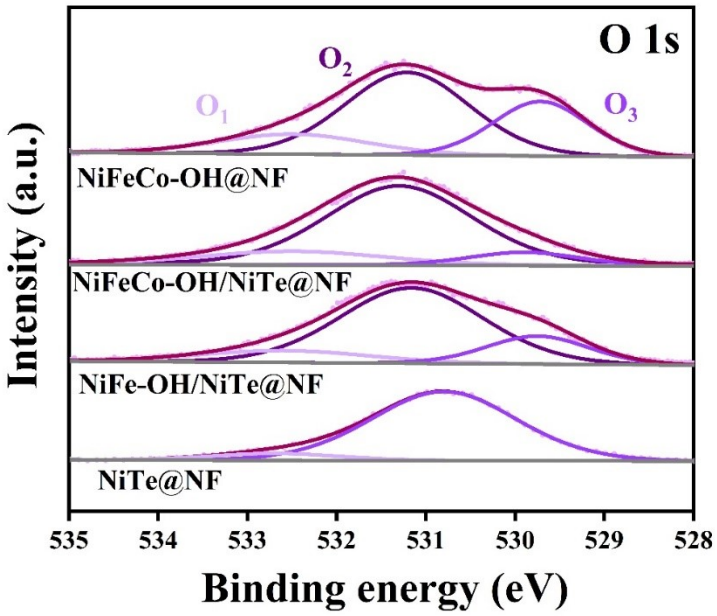

Fig. S9. High-resolution O 1s XPS spectra of NiFeCo-OH@NF, NiFeCo-OH/NiTe@NF, NiFe-OH/NiTe@NF and NiTe@NF.

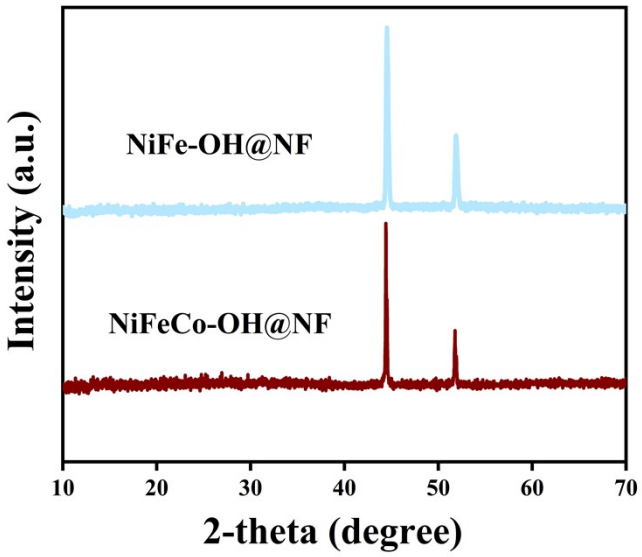

Fig. S10. XRD spectra of NiFe-OH@NF and NiFeCo-OH@NF.

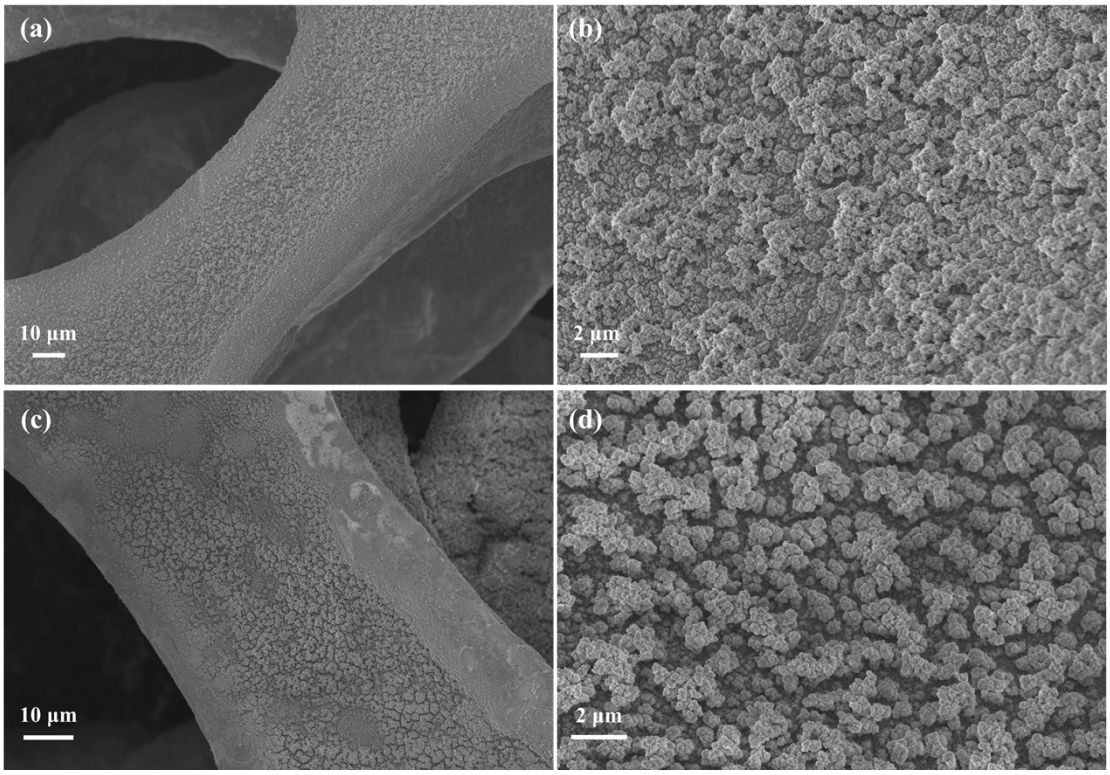

Fig. S11. FESEM images of (a) and (b) NiFeCo-OH@NF, (c) and (d) NiFe-OH@NF.

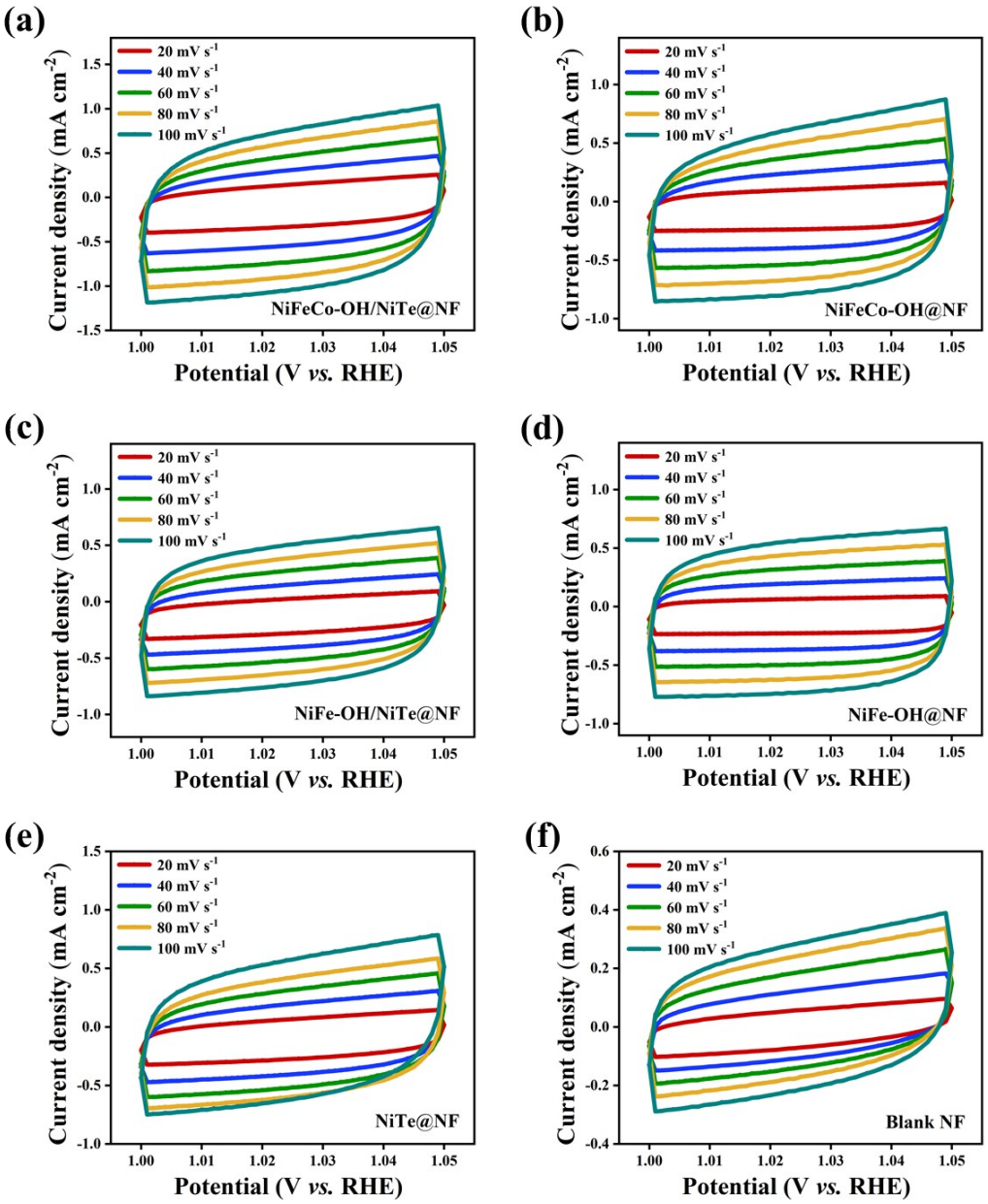

Fig. S12. CV curves of the as-prepared (a) NiFeCo-OH/NiTe@NF, (b) NiFeCo-OH@NF, (c) NiFe-OH/NiTe@NF, (d) NiFe-OH@NF, (e) NiTe@NF and (f) blank nickel foam recorded at different scan rates.

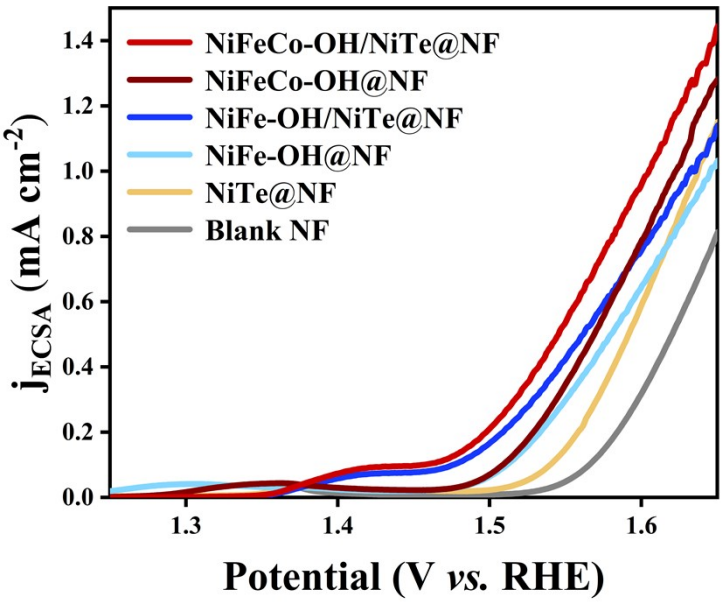

Fig. S13. ECSA-normalized LSV polarization curves.

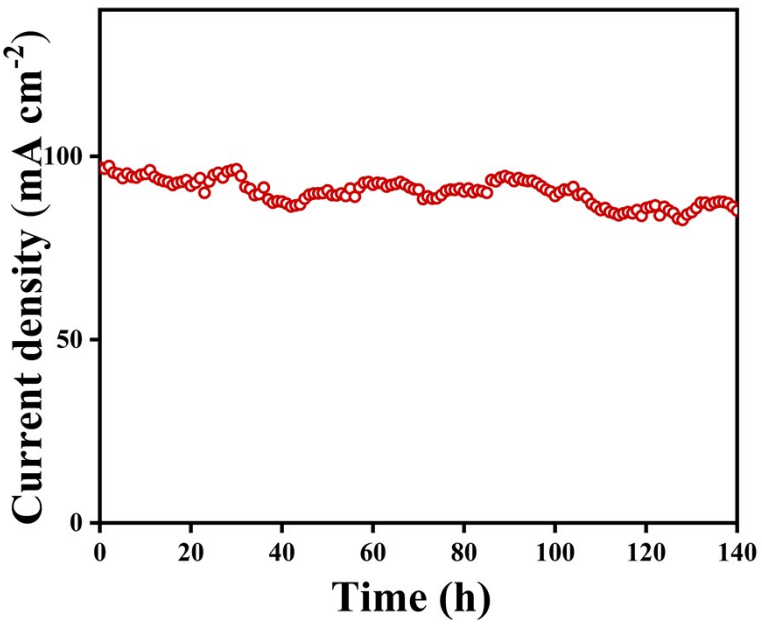

Fig. S14. Chronoamperometry curve of NiFeCo-OH/NiTe@NF at a constant potential of 1.52 V *vs.* RHE.

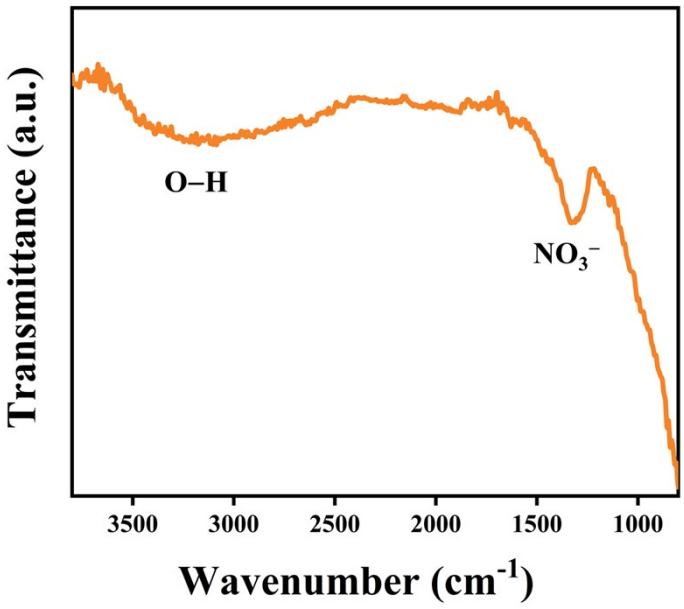

Fig. S15. FT-IR spectroscopy of NiFeCo-OH/NiTe@NF after the long-time chronoamperometry test for 45 h.

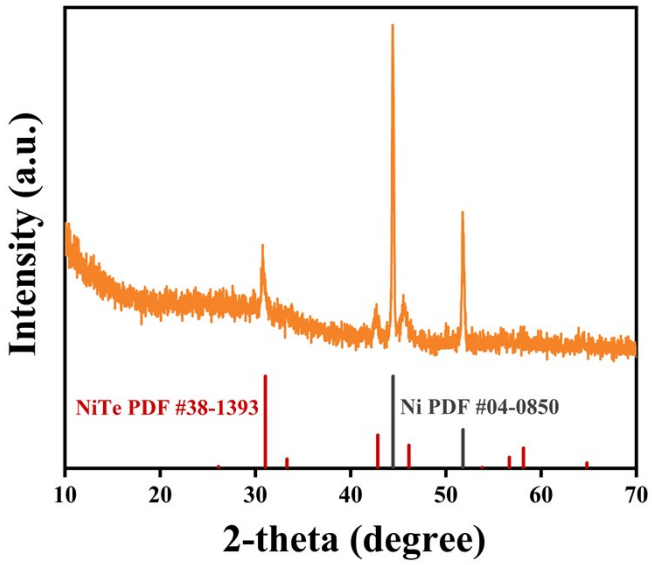

Fig. S16. XRD spectra of NiFeCo-OH/NiTe@NF after the long-time chronoamperometry test for 45 h.

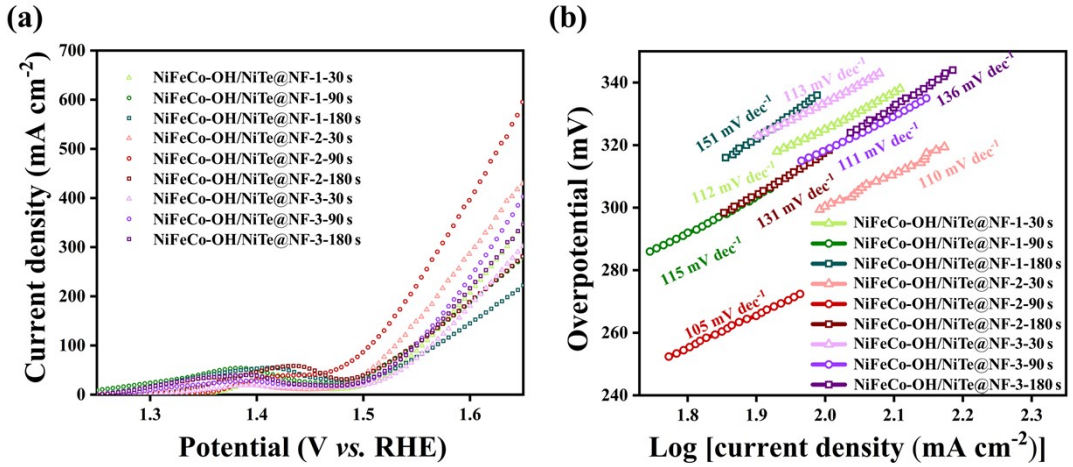

Fig. S17. (a) LSV curves and the derived (b) Tafel plots of NiFeCo-OH/NiTe@NF synthesized in different conditions.

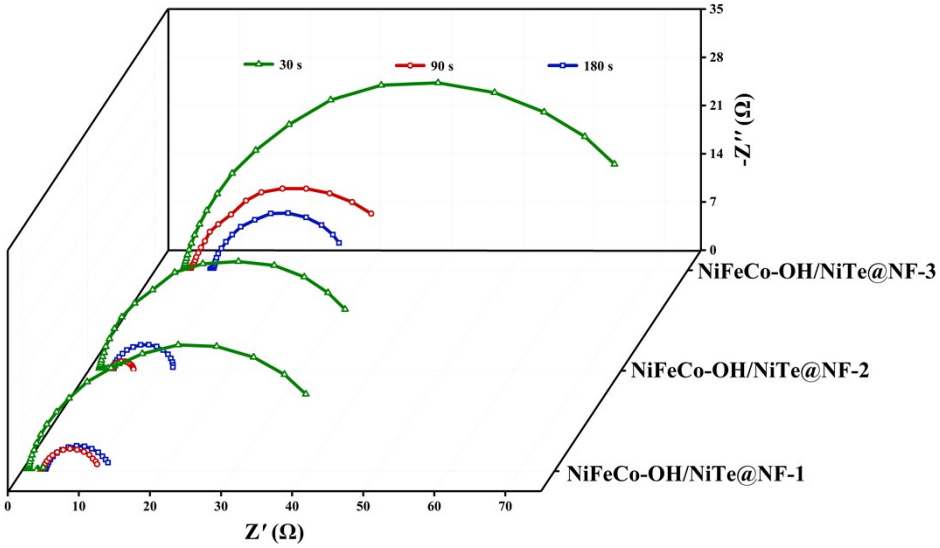

Fig. S18. EIS plots of NiFeCo-OH/NiTe@NF synthesized in different conditions.

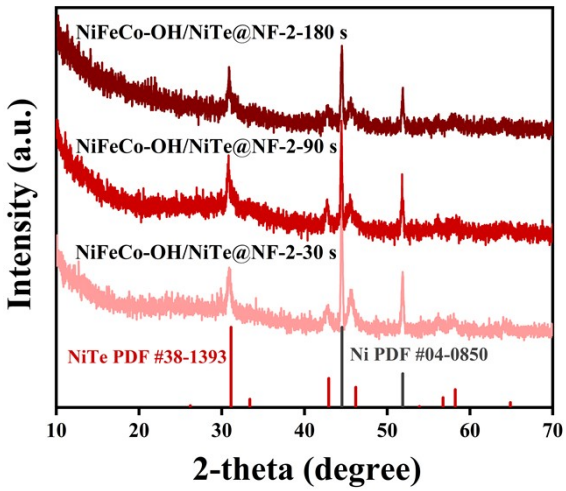

Fig. S19. XRD spectra of NiFeCo-OH/NiTe@NF-2 synthesized with different electrodeposition durations.

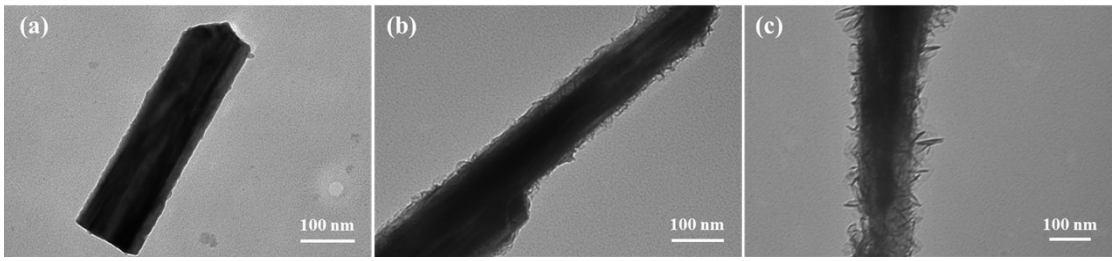

Fig. S20. TEM images of NiFeCo-OH/NiTe@NF-2 synthesized with different electrodeposition durations (a) 30 s, (b) 90 s, (c) 180 s.

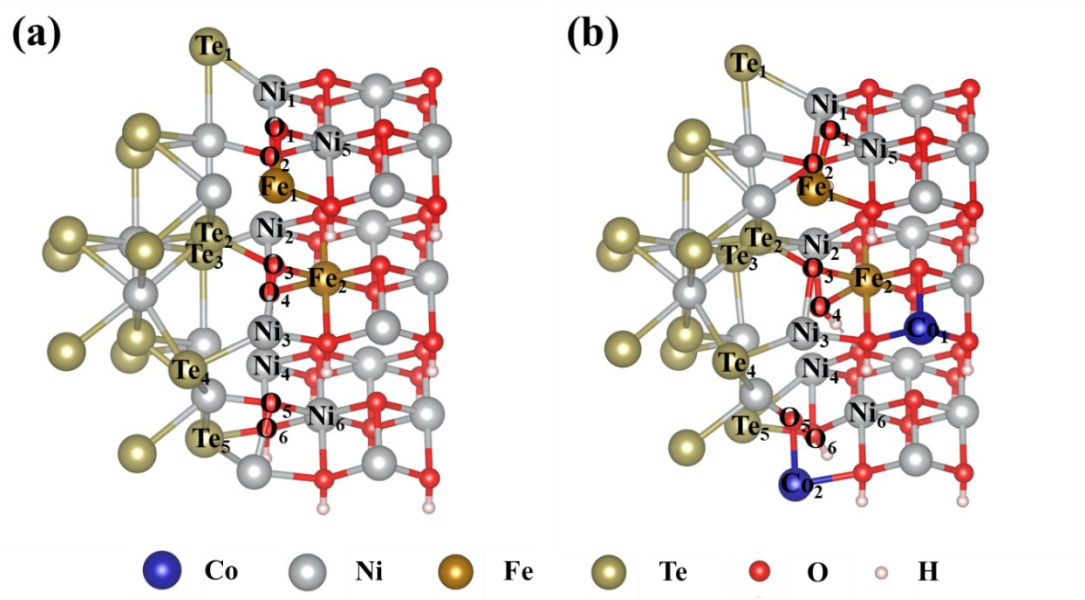

Fig. S21. Schematic of the model of (a) NiFe-OOH/NiTe, (b) NiFeCo-OOH/NiTe with Ni, Fe, Co, O, Te atoms numbered sequentially around the interface between oxyhydroxides and NiTe.

Table S1. ICP-AES analytical data for the mass fraction and mole fraction of Ni, Fe, Co, Te of the NiFeCo-OH/NiTe.

Element	Mass fraction (%)	Mole fraction (%)	Atomic ratio
Fe	0.7075	0.012679	1.7
Co	0.4386	0.0074423	1
Ni	34.8805	0.594287	80
Te	58.5393	0.45877	62

Table S2. Comparison of OER electrochemical performance of NiFeCo-OH/NiTe@NF with recently reported transition metal tellurides-based electrocatalysts.

Electrocatalysts	Electrolyte	Overpotential (mV, j = 100 mA cm^{-2})	Reference
NiTe/Ni_2P@NF	1.0 M KOH	310	S9
CoO@S-CoTe	1.0 M KOH	362	S10
Fe-NiTe-$Ni_{12}P_5$/NF	1.0 M KOH	323	S11
VTe_2@ZnFeTe/NF	1.0 M KOH	330	S12
Fe-$Co_{1.11}Te_2$@NCNTF	1.0 M KOH	388	S13
Cu_7Te_4 @CF	0.1 M KOH	409	S14
NiSe@CoTe	1.0 M KOH	286	S15
$CoTe_2$-$NiTe_2$	1.0 M KOH	299	S16
o-$CoTe_2$|P@HPC/CNTs	1.0 M KOH	287	S17
S-CoTe/CC	1.0 M KOH	318	S18
NiFeCo-OH/NiTe@NF	1.0 M KOH	276	This work

Table S3. The EIS calculation parameters of NiFeCo-OH/NiTe@NF, NiFeCo-OH@NF, NiFe-OH/NiTe@NF, NiFe-OH@NF, NiTe@NF and blank nickel foam.

Element	**R_s (Ω)**		**R_{ct} (Ω)**		**CPE-T (Ω)**		**CPE-P (Ω)**	
Sample	Value	Error (%)	Value	Error (%)	Value	Error (%)	Value	Error (%)
NiFeCo-OH/NiTe@NF	3.29	0.1406	3.28	0.8463	0.4936	1.0239	0.9130	0.7518
NiFeCo-OH@NF	3.11	0.3456	13.74	1.7195	0.2704	1.1250	0.8463	0.8910
NiFe-OH/NiTe@NF	3.87	0.1193	5.01	0.6739	0.3820	0.7088	0.8596	0.5557
NiFe-OH@NF	2.96	0.1733	15.46	1.5142	0.7028	0.7920	0.9137	0.4887
NiTe@NF	3.13	0.4085	129.90	2.1217	0.0707	0.6716	0.8714	0.4388
Blank NF	3.29	0.4742	185.30	2.4527	0.0430	0.8060	0.8579	0.4962

Table S4. The EIS calculation parameters of NiFeCo-OH/NiTe@NF synthesized in different conditions.

Element	R_s (Ω)		R_{ct} (Ω)		CPE-T (Ω)		CPE-P (Ω)	
Sample	Value	Error (%)	Value	Error (%)	Value	Error (%)	Value	Error (%)
NiFeCo-OH/NiTe-1-30 s	0.81	1.5086	47.85	4.5475	0.0847	2.1910	0.8268	1.2258
NiFeCo-OH/NiTe-1-90 s	2.80	0.6049	8.66	2.5743	0.2393	2.1701	0.8156	1.7300
NiFeCo-OH/NiTe-1-180 s	3.21	0.3883	9.73	1.7972	0.2165	1.5319	0.8283	1.2066
NiFeCo-OH/NiTe-2-30 s	1.57	0.4784	38.78	1.3626	0.0929	0.7833	0.8828	0.4845
NiFeCo-OH/NiTe-2-90 s	3.29	0.1406	3.28	0.8463	0.4936	1.0239	0.9130	0.7518
NiFeCo-OH/NiTe-2-180 s	3.40	0.2884	9.15	0.9327	0.1389	1.0531	0.8707	0.7368
NiFeCo-OH/NiTe-3-30 s	4.03	0.2216	68.27	0.6656	0.0490	0.3951	0.8607	0.2632
NiFeCo-OH/NiTe-3-90 s	5.04	0.3004	32.13	1.3934	0.1266	0.7643	0.8110	0.6308
NiFeCo-OH/NiTe-3-180 s	8.11	0.2463	19.84	1.2577	0.1660	1.0438	0.8858	0.7817

References

S1 X. Yu, M. Zhang, W. Yuan and G. Shi, *J. Mater. Chem. A*, 2015, **3**, 6921–6928.

S2 Z. Yan, H. Sun, X. Chen, H. Liu, Y. Zhao, H. Li, W. Xie, F. Cheng and J. Chen, *Nat. Commun.*, 2018, **9**, 2373.

S3 C. C. McCrory, S. Jung, J. C. Peters and T. F. Jaramillo, *J. Am. Chem. Soc.*, 2013, **135**, 16977–16987.

S4 G. Kresse and J. Furthmüller, *Phys. Rev. B,* 1996, **54**, 11169–11186.

S5 J. P. Perdew, K. Burke and M. Ernzerhof, *Phys. Rev. Lett.* 1996, **77**, 3865–3868.

S6 L. Peng, N. Yang, Y. Yang, Q. Wang, X. Xie, D. Sun-Waterhouse, L. Shang, T. Zhang and G. I. Waterhouse, *Angew. Chem. Int. Ed.,* 2021, **60**, 24612–24619.

S7 Y. Ma, Y. Ma, Q. Wang, S. Schweidler, M. Botros, T. Fu, H. Hahn, T. Brezesinski and B. Breitung, *Energy Environ. Sci.*, 2021, **14**, 2883–2905.

S8 Z. W. Seh, J. Kibsgaard, C. F. Dickens, I. B. Chorkendorff, J. K. Nørskov and T. F. Jaramillo, *Science,* 2017, **355**, 146.

S9 M. Xing, Z. Qiao, Z. Niu, S. Wang, Z. Liu and D. Cao, *ACS Appl. Mater. Interfaces*, 2023, **15**, 40428–40437.

S10 X. Wang, Z. Mao, X. Mao, X. Hu, F. Gao, M. Gao, Q. L. Wu, X. Lyu, A. Du, X. Xu, Y. Jia and L. Wang, *Adv. Sci.*, 2023, **10**, e2206204.

S11 Y. Tang, Y. Zou and D. Zhu, *J. Mater. Chem. A*, 2022, **10**,12438–12446.

S12 J. Gautam, D. Chanda, M. M. Meshesha, S. G. Jang and B. L. Yang, *Chem. Eng. J.*, 2023, **467**, 143535.

S13 B. He, X. C. Wang, L. X. Xia, Y. Q. Guo, Y. W. Tang, Y. Zhao, Q. L. Hao, T. Yu, H. K. Liu and Z. Su, *ChemSusChem*, 2020, **13**, 5239–5247.

S14 R. Wang, Y. Liu, Z. Tian, Y. Shi, Q. Xu, G. Zhang, J. Chen and W. Zheng, *J.*

Phys. Chem. C, 2020, **124**, 22117–22126.

S15 D. A. Alshammari, Y. M. Riyad, S. Aman, N. Ahmad, H. M. Tahir Farid and Z. M. El-Bahy, *J. Electroanal. Chem.*, 2023, **945**, 117701.

S16 Y. Qi, Z. Yang, S. Peng, Y. Dong, M. Wang, X.-Q. Bao, H. Li and D. Xiong, *Inorg. Chem. Front.*, 2022, **9**,332–342.

S17 Z. Chen, M. Chen, X. Yan, H. Jia, B. Fei, Y. Ha, H. Qing, H. Yang, M. Liu and R. Wu, *ACS Nano*, 2020, **14**, 6968–6979.

S18 L. Yang, H. Qin, Z. Dong, T. Wang, G. Wang and L. Jiao, *Small*, 2021, **17**, e2102027.